Tsunetomo Yamada*,**, Gaston Garbarino, Hiroyuki Takakura, Cesar Pay Gòmez, Ryuji Tamura and Marc de Boissieu*

In-situ high-pressure X-ray diffraction on the Zn_6Sc $^1/_1$ periodic cubic approximant to a quasicrystal

Abstract: The Zn_6Sc $^1/_1$ cubic approximant to a quasicrystal has been studied *in-situ* at high pressures by single-crystal X-ray diffraction. This phase can be described as a bcc packing of Tsai-type icosahedral clusters whose center is occupied by a disordered Zn_4 tetrahedron. At ambient pressure the Zn_6Sc undergoes a structural phase transition at 159 K to a monoclinic superstructure in which the Zn_4 tetrahedra are orientationally ordered along the [$\bar{1}$01] direction of the high-temperature bcc phase. In the pressure range up to 35 GPa, two new superstructures have been observed. The second phase corresponds to a four-fold pseudo cubic superstructure, i.e. a very large unit cell with a lattice parameter of about 5.5 nm. The resulting pressure-temperature phase diagram is different from that of Cd_6Yb, which was reported by Watanuki et al. (2006).

Keywords: quasicrystals, approximants, phase transition

*Corresponding Authors: Tsunetomo Yamada, Marc de Boissieu, Department of Materials Science and Technology, Tokyo University of Science, Noda, 278-8510, Japan; Sciences et Ingèenierie des Matèriaux et Procèès, Grenoble-INP,CNRS, UJF, BP 75 38402, St Martin d'HéresCedex, France; e-mail: tntmymd@tagen.tohoku.ac.jp, Marc.de-boissieu@simap.inpg.fr
**Current address: Institute of Multidisciplinary Research for Advanced Materials (IMRAM), Tohoku University, Katahira 2-1-1, Aoba-ku, Sendai 980-8577, Japan
Gaston Garbarino: European Synchrotron Radiation Facility, BP 220, 38043 Grenoble, France
Hiroyuki Takakura: Division of Applied Physics, Graduate School of Engineering, Hokkaido University, Sapporo, 060-8628, Japan
Cesar Pay Gòmez: Department of Chemistry, Ängström Laboratory, Uppsala University, Uppsala, 751 05, Sweden
Ryuji Tamura: Department of Materials Science and Technology, Tokyo University of Science, Noda, 278-8510, Japan

Introduction

Quasicrystals [1] are long-range ordered structures which lack lattice periodicity (for an introduction see [2]). Recent progress has been achieved in understanding their atomic structure [3] and physical properties [4] thanks to discoveries of a stable *i*-$Cd_{5.7}Yb$ [5] binary icosahedral phase and an isostructural *i*-$Zn_{80}Mg_5Sc_{15}$ phase [6]. In both systems, the quasicrystal and its periodic approximant can be synthesized with almost the same chemical composition [7, 8]. As shown recently [3], their structures can be described as a packing of the same large rhombic triacontahedral (RTH) unit, consisting of 158 atoms arranged on successive shells with pseudo icosahedral symmetry, surrounding the central, symmetry-breaking tetrahedron (Fig. 1a). The RTH units in the quasicrystal (QC hereafter) and in the 1/1 cubic approximant are connected along their twofold axes by shared faces and they overlap along their threefold axes. While in the 1/1 approximant they are located on the vertices of a bcc lattice with space group $Im\bar{3}$ (lattice parameter $a = 1.57$ and 1.38 nm for Cd_6Yb and Zn_6Sc, respectively), in the QC the RTH units are arranged on the vertices of a quasiperiodic network.

In most Cd_6RE (RE stands for rare earth element) phases, an order-disorder type transition has been observed [9, 10] and attributed to the orientational ordering of the central tetrahedron. The most detailed structural information has been obtained for the Zn_6Sc cubic phase for which the order-disorder phase transition (T_c) is 160 K [11–14]. Above T_c, in the Zn_6Sc 1/1 approximant, and similar to the Cd_6RE 1/1 approximant, the central tetrahedron appears orientationaly disordered, randomly occupying six orientations that are equivalent under the cubic symmetry [7, 8]. At 160 K, the high temperature (HT) cubic phase of Zn_6Sc transforms to a low-temperature (LT) monoclinic phase with space group $C2/c$, in which the Zn_4 tetrahedra are ordered and oriented antiparallel along the [$\bar{1}$01] direction [11, 13, 14], as depicted in Fig. 1b. The LT structure analysis [13, 14] showed that

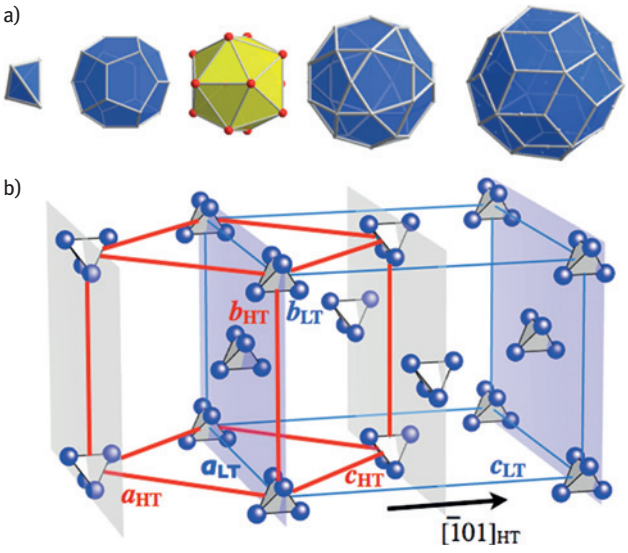

Fig. 1: (a) Icosahedral cluster, consisting of five successive shells: From the center: tetrahedron, dodecahedron, icosahedron, icosidodecahedron and rhombic triacontahedron. (b) Schematic representation of the ordering scheme of the tetrahedral along the [$\bar{1}$01] direction of the HT cubic phase. The two different planes parallel to ($\bar{1}$01) are highlighted with different colors. The HT and LT lattice basis vectors satisfy following relations, $\boldsymbol{a}_{LT} = \boldsymbol{a}_{HT} + \boldsymbol{c}_{HT}$, $\boldsymbol{b}_{LT} = \boldsymbol{b}_{HT}$, $\boldsymbol{c}_{LT} = -\boldsymbol{a}_{HT} + \boldsymbol{c}_{HT}$.

the orientational ordering of the central Zn_4 tetrahedron induces a strong distortion of the successive shells around it, which therefore depart significantly from perfect icosahedral symmetry, as exemplified for the dodecahedral shell in Fig. 1a. This is confirmed by molecular dynamics (MD) simulations with oscillating pair potentials that also reproduce the phonon spectra in this phase [4]. Moreover, using quasielastic neutron scattering [15] and atomic-scale MD simulations [15, 16], it has been shown that the Zn tetrahedron behaves as a single 'molecule' that reorients dynamically above T_c, conferring an unique 'dynamical flexibility' to the Zn_6Sc. Finally, there is evidence for short-range order of the tetrahedra above T_c. Although the phase transition is first order, all of these results are consistent with a 'weak' first order transition, mainly driven by the ordering of the tetrahedra [13]. A similar dynamical flexibility was observed in the quasicrystal [17] , although in that case the freezing of the tetrahedra occurs progressively, as in a glassy system.

Watanuki et al. (2006) have investigated the phase diagram of Cd_6Yb at simultaneous LT and high-pressures and observed five new superstructure schemes, labeled from I to V, as a function of the applied pressure up to 5.2 GPa [18]. They found that the ordering scheme is sensitive to the temperature and pressure: at ambient pressure the LT superstructure (phase I) has a propagation vector along [110] direction of the HT phase, breaking the cubic symmetry. At 1.0 GPa it transforms to a cubic superstructure (phase III) with ordering along ⟨111⟩. Because of this phase has cubic symmetry, the propagation vector is [111] and all the equivalents. When T increases up to 250 K, two phases appear as HT phase (III' and II). The phase III transforms to a superstructure with [110]-type ordering (phase V) as P increases to 3.5 GPa. The phase V transforms to two superstructures IV and IV' when T increases.

Nozawa et al. compared the crystal structures of the Zn_6Sc and Cd-based cubic 1/1 approximants at high pressure using a first-principles calculation [19–21] and predicted that the P–T phase diagram of Zn_6Sc differs from Cd_6Yb [21]. It is therefore of interest to understand the structural modifications of these phases under pressure, as they may shed some light on the tetrahedron-tetrahedron interaction, an important parameter to understand the stabilization mechanisms of both the quasicrystals and their approximants. In this paper, we present a detailed *in-situ* single-crystal X-ray diffraction study, at LT and under high pressure up to 35 GPa, of the Zn_6Sc $^1/_1$ approximant.

Experimental details

Single grained samples of the Zn_6Sc $^1/_1$ cubic approximant have been synthesized by slow cooling from the melt (see [12] for details). It is known that the phase transition in Zn_6Sc becomes sluggish or even vanishes depending on the details of sample preparation [12, 14]. The sample we measured in this experiment was well characterized and exhibits very sharp anomalies in both electrical resistivity and heat capacity at 157 K under ambient pressure as depicted in Fig. 2.

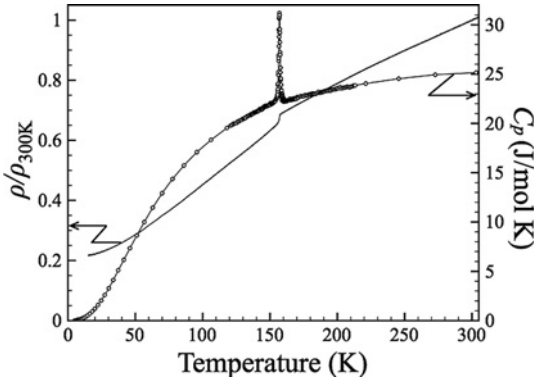

Fig. 2: Temperature dependence of electrical resistivity and heat capacity of Zn_6Sc.

In-situ single-crystal X-ray diffraction experiments were conducted at the ID27 beamline of the European Synchrotron Radiation Facility (ESRF). High brilliance synchrotron radiation from a two-phased undulator was set to a wavelength of 0.3738 Å using a Si(111) monochromator. The X-ray beam was focused down to $3 \times 4\,\mu m^2$ using two mirrors and Kirkpatrick–Baez (K–B) mirrors. The single grained sample of Zn_6Sc was crushed and some pieces with a diameter between 40 and 90 µm were chosen and mounted in a diamond anvil cell (DAC), together with a small ruby ball. Helium was used as a pressuure-transmitting medium. The DAC was set inside a home-made low-temperature helium flow cryostat. Single-crystal X-ray diffraction patterns were collected using a MAR 165 CCD detector. The detector was located about 345 mm away from the sample. Measurements were carried out with an rotation of the sample is, for single crystal measurements, termed an omega scan, with step size of 1.0°. Pressure was determined *in-situ* from the calibrated shift of the ruby R_1 fluorescent line. The data processing was carried out using the CrysAlisPro computer program (Agilent Technologies) [22].

We explored the P–T phase diagram with the following procedure. At ambient pressure, we first detected the phase transition at 159 K by observing the splitting of Bragg peaks and the appearance of superstructure reflections. We then increased P at a constant T equal to 180 K, i.e. 20 K above T_c. For each pressure we carefully looked for phase transition. At several pressures up to 35 GPa we carried out temperature scans to track down possible transitions and new phases.

Results and discussions

Figure 3 shows the P-dependence of the cubic cell volume, where the cubic lattice constant was estimated from the diffraction data using CrysAlisPro. By a least-squares fit using the third order Brich-Murnaghan equation of state we found the zero-pressure bulk modulus, B_0, and its pressere derivative, B_0', for the Zn_6Sc to be equal to 85.2 GPa and 4.6, respectively. The value B_0 is slightly larger than that found in the Zn–Mg–Y icosahedral quasicrystal ($B_0 = 73 \pm 1$ GPa) [23] and pure Zn element (68.3 GPa) [24]. On the other hand, B_0 is about twice as large as that of Cd_6Yb (46.1 GPa) [25].

During the P–T study we observed two types of diffraction patterns which differ from the LT monoclinic superstructure observed at ambient pressure. The differences are clearly apparent in the zero and 1st layers of the reconstructed reciprocal lattice (Fig. 4). Hereafter, we

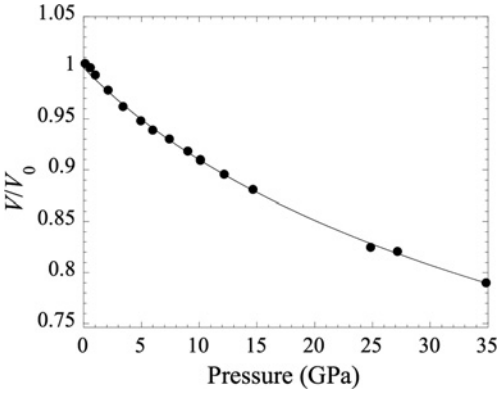

Fig. 3: Pressure dependence of the normalized volumes of Zn_6Sc.

call the LT superstructure at ambient pressure phase A, and the two new phases as phase B and C, respectively. The characteristics of their superstructures are illustrated in Fig. 5.

Below T_c at ambient pressure the diffraction pattern is found to be identical to the previous single-crystal X-ray diffraction experiment [13]. This confirms that phase A is the $C2/c$ monoclinic superstructure with a doubled unit cell with parameters equal to $\sqrt{2}\boldsymbol{a}_{HT} \times \boldsymbol{a}_{HT}$

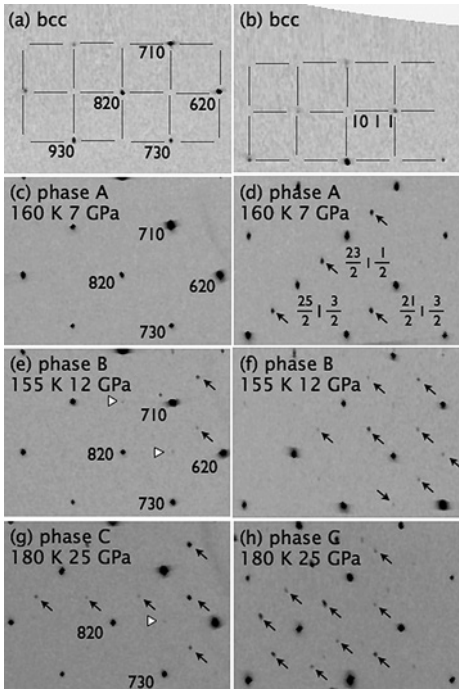

Fig. 4: Reconstructed reciprocal layers from single-crystal X-ray diffraction data of Zn_6Sc. (a) $k = 0$ and (b) $k = 1$ layer of HT bcc phase. (c) $k = 0$ and (d) $k = 1$ layer of phase A obtained at 160 K at 7.8 GPa. (e) $k = 0$ and (f) $k = 1$ layer of phase B at 155 K at 14.3 GPa (g) $k = 0$ and (h) $k = 1$ layer of phase C at 180 K at 26.7 GPa. Arrows denote superstructure reflections. Some weak reflections indicated by open arrow heads cannot be indexed.

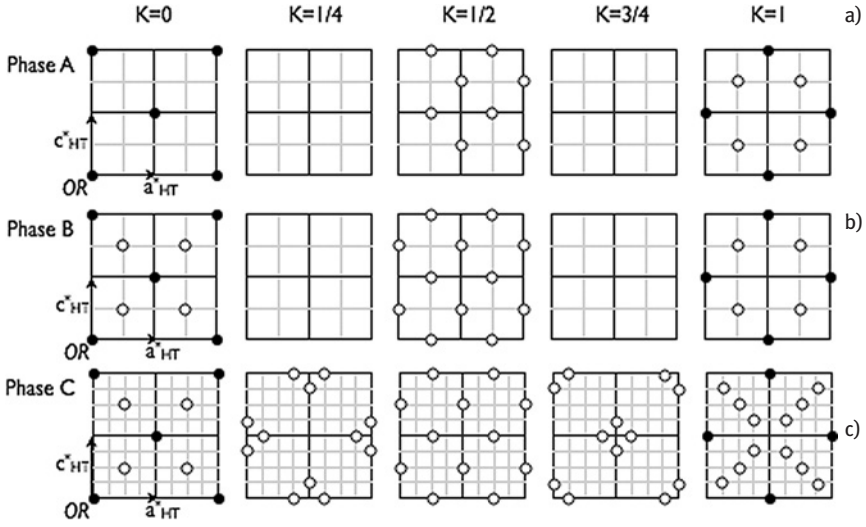

Fig. 5: Illustrations of the reciprocal lattice corresponding to (a) phase A, (b) phase B and (c) phase C. Solid and open symbols indicate main and superstructure reflections, respectively. OR denotes the origin of the reciprocal lattice.

$\times \sqrt{2}\boldsymbol{a}_{HT}$, where $\boldsymbol{a}_{HT}$ is the HT cubic lattice. This arises from anti-parallel ordering along the $[\bar{1}01]$ direction of the HT phase. Here we note that superstructure reflections are observed not only at the position $h_{HT} - ½$, k_{HT}, $l_{HT} + ½$ but also at other positions e.g. h_{HT}, $k_{HT} - ½$, $l_{HT} - ½$ and $h_{HT} - ½$, $k_{HT} - ½$, l_{HT}, where h_{HT}, k_{HT} and l_{HT} are indices of the HT phase. This can be explained by a fact that the transition leads to six different domains [13]. Hence the observed diffraction pattern shows a superposition of diffraction spots from the six domains. Consequently, the superstructure reflections appear at the position $h_{HT} - ½$, k_{HT}, $l_{HT} + ½$ and its permutations corresponding to the six variants [13]. If we compare the intensities of the equivalent superstructure reflections, it can be noticed that some superstructure reflections are weak or even absent in Fig. 4. This indicates that the volume fraction of some of the six domains are larger than others.

This phase A has also been observed at $(P, T) =$ (7.8 GPa, 160 K), as can be seen in Fig. 4c and d. At this pressure the volume compression is already significant (10%), yet T_c is within 20 K of the transition temperature measured at ambient pressure.

At $(P, T) =$ (12.3 GPa, 180 K) we observed a diffraction pattern corresponding to the HT bcc phase. When we decrease T below 155 K at 14.3 GPa, we observed new superstructure reflections appearing at the positions $h_{HT}/2$, 0, $l_{HT}/2$ on the zero layer, which distinguishes this phase from the phase A. In addition, we noticed that no reflection appears at the position $h_{HT}00$, where $h_{HT} =$ odd, and its cubic cyclic permutations. These facts cannot be explained by simple doubling of the cubic unit cell, because no cubic space group satisfies such an extinction rule ($h00$; $h \neq 4n$, n integer). Therefore, this new phase has an orthorhombic or lower symmetry, which forms several orientational domains. This makes the interpretation of the diffraction pattern rather complicated, in the same way as for the transition from HT bcc phase to phase A. However, if we assume a new superstructure with $\boldsymbol{q}$-vector of $(\boldsymbol{a}^*_{HT} - \boldsymbol{c}^*_{HT})/2$, all observed superstructure reflections can be indexed with a unit cell $\sqrt{2}\boldsymbol{a}_{HT} \times \boldsymbol{a}_{HT} \times \sqrt{2}\boldsymbol{a}_{HT}$ and its variants with different orientations. When we increased T to 180 K at this pressure we observed diffraction patterns which correspond to the HT bcc phase.

At $(P, T) =$ (26.7 GPa, 180 K) we observed new superstructure reflections at position $h_{HT}/4$, $k_{HT}/4$, $l_{HT}/4$, which can be interpreted with a four-fold cubic superstructure with a huge lattice parameter of about 5.5 nm. No superstructure reflections appear at positions $h_{HT}00$ where $h_{HT} =$ odd, and its cubic cyclic permutations. Therefore, the superstructure reflections cannot be explained simply by this four times larger cubic unit cell, because no cubic lattice satisfies such an extinction rule ($h00$; $h \neq = 8n$, n is integer), where h is index h of the four times cubic supercell. Hence the phase C has a non-cubic unit cell. In the same way as for the previous two cases, this lower symmetry results in a formation of different domains and it is a challenge to determine the structure. If we assume a $\boldsymbol{q}$-vector equal to $(3\boldsymbol{a}^*_{HT} - \boldsymbol{c}^*_{HT})/4$, superstructure reflections can be indexed as first-, second- and third-order superstructure reflections, as depicted in Fig. 6. Figure 6a shows main, first-, second- and third-order superstructure reflections on the 1st layer ($k = 1$) from a variant. With this $\boldsymbol{q}$-vector the symmetry is monoclinic or lower and the mirror symmetry perpendicular to $\boldsymbol{a}^*_{HT}$ axis is broken. Therefore diffraction spots from another variant in the mirror symmetry (Fig. 6b) are superimposed. The resulting simulated diffraction pattern (Fig. 6c) reproduces the observed pattern as shown in Fig. 4h. The same

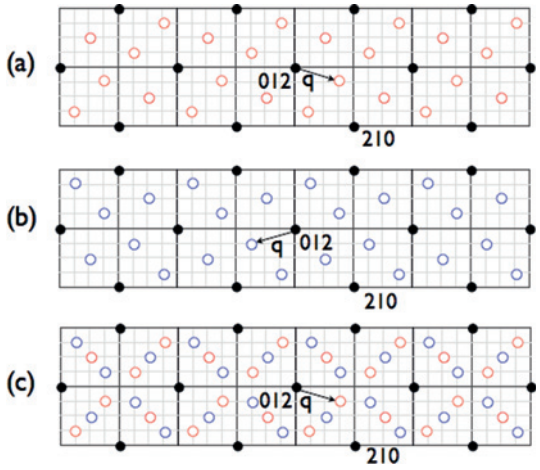

Fig. 6: Diffraction spots on a reciprocal layer ($k = 1$) with a $\boldsymbol{q}$-vector equal to $(3\boldsymbol{a}^*_{HT} - \boldsymbol{c}^*_{HT})/4$. Solid and open circles are main and superstructure reflections, respectively. (a) Diffraction pattern from a single variant. (b) Diffraction spots from a single variant which mirror twin of (a). (c) Superimposed diffraction spots of (a) and (b).

diffraction pattern has been observed up to 250 K at the same pressure, without any phase transition, and was also observed at (P, T) = (34.8 GPa, 180 K).

All of these results are summarized on a P-T phase diagram in Fig. 7. The phase A appears for a transition temperature between 160 K and 180 K below 7.8 GPa. We notice that up to 10 GPa, the transition temperature leading to the $C2/c$ structure is almost independent of pressure, although in this range the volume compression $(V - V_0)/V_0$ is 10%. Phase C has been observed at pressures at or above 26.8 GPa. Because of the experimental conditions it was impossible to measure data between 14.3 and 26.8 GPa. The phase C has been observed up to 250 K at 24.3 GPa. It is thus unclear whether this phase will transform to the $Im\bar{3}$ cubic phase at higher T.

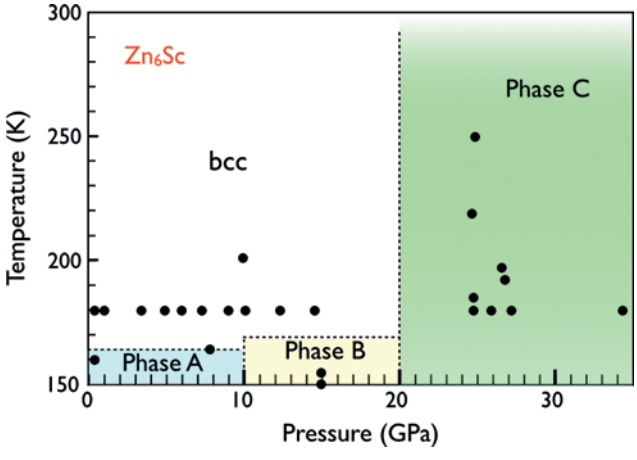

Fig. 7: Pressure-temperature phase diagram of Zn_6Sc. The solid symbols are experimental points.

The resulting P–T phase diagram obtained for Zn_6Sc is different from that obtained for Cd_6Yb [17]. Cd_6Yb shows a rich series of phase transitions, with five different superstructure phases in the narrow P range up to 5.2 GPa, whereas Zn_6Sc shows only three superstructures in the wider P range up to 34.8 GPa. In addition, the ordering schemes of the tetrahedra in Zn_6Sc are different from those in Cd_6Yb. The ⟨111⟩-type superstructure which was observed in Cd_6Yb at the P range between 1 and 3 GPa, was not observed in Zn_6Sc.

In our investigation on Zn_6Sc, $\boldsymbol{q}$-vectors were found to be $(\boldsymbol{a}^*_{HT} - \boldsymbol{c}^*_{HT})/2$ and $(3\boldsymbol{a}^*_{HT} - \boldsymbol{c}^*_{HT})/4$ for the phases B and C, respectively. In phase B the lattice and $\boldsymbol{q}$-vector are the same as the LT monoclinic superstructure (phase A), hence phase A can be regarded as a prototype structure of phases B and C. The modifications of the tetrahedral order in phase B with those $\boldsymbol{q}$-vectors can be fulfilled by rotating the tetrahedra around the b-axis, i.e the unique axis of the monoclinic cell, because the rotation angle of the tetrahedron around the b-axis is unrestricted by the symmetry.

Because the bulk modulus of the Zn_6Sc phase is twice as large as that of Cd_6Yb, it is expected that the ordering transitions of Zn_6Sc are less sensitive to P as compared to Cd_6Yb. Indeed we find that the transition from cubic to monoclinic (phase A) occurs for essentially the same T_c from ambient pressure up to 7.8 GPa. Then a new phase (phase B) appears in the P range between 7 and 12 GPa with the compression ratio equal to about 10%. In the Cd_6Yb the phase I transforms to phase III at 1 GPa with a compression ratio equal to only 1% [18]. Such a difference can not be explained solely by considering the differences in bulk moduli. Another important difference to be pointed out is the mixed valence character of Yb atoms [26]. Nozawa and Ishii [19–21] have investigated the P dependence of the tetrahedral configurations using a first-principles density-functional calculation. As these authors described, configurational stability of the tetrahedral ordering and its P dependence depends on valence of the second elements i.e. divalent (Ca and Yb) and trivalent (Sc and Y). They showed that there are significant differences in the potential energy surfaces (PES) for tetrahedral rotation (θ) around the two-fold axis between the Cd_6Yb and Zn_6Sc phases as a function of P and T. The different behavior observed experimentally under pressure is certainly related to these differences in the PES. The present results constitute thus provide a valuable contribution to constraining the nature of the subtle tetrahedron-tetrahedron interaction at play in these compounds. The details of this long-range interaction (about 1.3 nm) is mediated by the successive

distortion of the surrounding shells on one hand and by the Zn(Cd)–Sc(Yb) hybridization on the other hand. Those are important parameters in the understanding of the mechanisms stabilizing both the quasicrystal and their respective periodic approximants.

Acknowledgements: We thank the ESRF for the allocation of beam time.

References

[1] Shechtman, D.; Blech, I.; Gratias, D.; Cahn, J. W.: Metallic phase with long-range orientational order and no translational symmetry. Phys. Rev. Lett. **53** (1984) 1951–1953.

[2] Janssen, T.; Chapuis, G.; de Boissieu, M.: Aperiodic Crystals. From modulated phases to quasicrystals. IUCr Monographs on Crystallography, No. 20, Oxford: IUCr/Oxford University Press (2007).

[3] Takakura, H.; Pay Gòmez, C.; Yamamoto, A.; de Boissieu, M.; Tsai, A. P.: Atomic structure of the binary icosahedral Yb–Cd quasicrystal. Nature Materials **6** (2007) 58–63.

[4] de Boissieu. M.; Francoual, S.; Mihalkovič, M.; Shibata, K.; Baron, A. Q. R.; Sidis, Y.; Ishimasa, T.; Wu, D.; Lograsso, T.; Regnault, L. P.; Gähler, F.; Tsutsui, S.; Hennion, B.; Bastie, P.; Sato, T. J.; Takakura, H.; Currat, R.; Tsai, A. P.: Lattice dynamics of the Zn–Mg–Sc icosahedral quasicrystal and its Zn–Sc periodic 1/1 approximant. Nature Materials **6** (2007) 977–984.

[5] Tsai, A. P.; Guo, J. Q.; Abe, E.; Takakura, H.; Sato, T. J.: A stable binary quasicrystal. Nature **408** (2000) 537–538.

[6] Kaneko, Y.; Arichika, Y.; Ishimasa, T.; Icosahedral quasicrystal in annealed Zn–Mg–Sc alloys. Phil. Mag. Lett. **81** (2001) 777–787.

[7] Pay Gòmez, C.; Lidin, S.: Comparative structural study of the disordered MCd_6 quasicrystal approximants. Phys. Rev. B **68** (2003) 024203.

[8] Lin, Q. S.; Corbett, J. D.: Synthesis and structure of five $Sc_3Cu_yZn_{18-y}$ type compositions ($0 < y < 2.2$), 1/1 crystalline approximants of a new icosahedral quasicrystal. Direct example of tuning on the basis of size effects and Hume-Rothery concepts. Inorg. Chem. **43** (2004) 1912–1919.

[9] Tamura, T.; Murao, Y.; Takeuchi, S.; Ichihara, M.; Isobe, M.; Ueda, Y.: A low-temperature order-disorder transition in a cubic Cd_6Yb crystalline approximant. Jpn. J. Appl. Phys. **41** (2002) L524–L526.

[10] Tamura, R.; Edagawa, K.; Aoki, C.; Takeuchi, S.; Suzuki, K.: Low-temperature structural phase transition in a Cd_6Y 1/1 approximant. Phys. Rev. B **68** (2003) 174105.

[11] Tamura, R.; Nishimoto, K.; Takeuchi, S.; Edagawa, K.; Isobe, M.; Ueda, Y.: Universal low-temperature phase transition in Zn- and Cd-based crystalline approximants. Phys. Rev. B **71** (2005) 092203.

[12] Yamada, T.; Tamura, R.; Muro, Y.; Motoya, K.; Isobe, M.; Ueda, Y.: Experimental evidence for a phase transition in a Zn_6Sc 1/1 cubic approximant. Phys. Rev. B **82** (2010) 134121.

[13] Yamada, T.; Euchner, H.; Pay Gòmez, C.; Takakura, H.; Tamura, R.; de Boissieu, M.: Short- and long-range ordering during the phase transition of the Zn_6Sc 1/1 cubic approximant. J. Phys.: Condens. Matter **25** (2013) 205405.

[14] Ishimasa, T.; Kasano, Y.; Tachibana, A.; Kashimoto, S.; Osaka, K.: Low temperature phase of the Zn–Sc approximant. Phil. Mag. **87** (2007) 2887–2897.

[15] Euchner, H.; Yamada, T.; Schober, H.; Rols, S.; Mihalkovič, M.; Tamura, R.; Ishimasa, T.; de Boissieu, M.: Ordering and dynamics of the central tetrahedron in the 1/1 Zn_6Sc periodic approximant to quasicrystal. J. Phys.: Condens. Matter **24** (2012) 415403.

[16] Mihalkovič, M.; Henley, C. L.: Energetics and dynamics of caged Zn_4 in *i*-ScZn, Phil. Mag. **91** (2010) 2548–2556.

[17] Euchner, H.; Yamada, T.; Rols, S.; Ishimasa, T.; Kaneko, Y.; Ollivier, J.; Schober, H.; Mihalkovič, M.; de Boissieu, M.: Tetrahedron dynamics in the icosahedral quasicrystals *i*-ZnMgSc and *i*-ZnAgSc and the cubic 1/1-approximant Zn_6Sc. Journal of Physics-Condensed Matter, **25** (2013) 115405.

[18] Watanuki, T.; Machida, A.; Ikeda, T.; Aoki, K.; Kaneko, H.; Shobu, T.; Sato, T. J.; Tsai, A. P.: Pressure-Induced Phase Transitions in the Cd–Yb Periodic Approximant to a Quasicrystal. Phys. Rev. Lett. **96** (2006) 105702.

[19] Nozawa, K.; Ishii, Y.: First-principles studies for structural transitions in ordered phase of cubic approximant Cd_6Ca. Journal of Physics: Condensed Matter **20** (2008) 315206.

[20] Nozawa, K.; Ishii, Y.: First-principles study for phase diagrams of Cd–Ca and Cd–Y Tsai-type approximants under pressure. Aperiodic Crystals, Springer Netherlands (2013) 195–201.

[21] Hatakeyama, T.; Nozawa, K.; Ishii, Y.: Ab-initio studies on orientational ordering in cubic Zn–Sc. Zeitschrift für Kristallographie **223** (2008) 830–832.

[22] CrysAlisPro, Version 1.171.35.6, Agilent Technologies Ltd, Yarnton England, (2011).

[23] Hasegawa, M.; Tsai, A. P.; Yagi, T.: Journal of Physics: Conference Series **92** (2007) 012184.

[24] Simmons, G.; Wang, H.: Single Crystal Elastic Constants and Calculated Aggregate Properties 2nd ed. M.I.T. Press, New York (1971).

[25] Watanuki, T.; Sato, T. J.; Tsai, A. P.: Structural stability of an icosahedral Cd-Yb quasicrystal and its crystalline approximant under high pressure. Journal of Physics: Conference Series **215** (2010) 012019.

[26] Kawana, D.; Watanuki, T.; Machida, A.; Shobu, T.; Aoki, K.; Tsai, A. P.: Intermediate-valence quasicrystal of a Cd–Yb alloy under pressure, Phys. Rev. B **81** (2010) 220202(R).

Received August 5, 2013; accepted November 4, 2013
Published online January 9, 2014